CF_4/H_2 Plasma Cleaning of Graphene Regenerates Electronic Properties of the Pristine Material

Djawhar Ferrah,[†,‡,*] Olivier Renault,[†] Daniil Marinov,[§] Javier Arias-Zapata,[†,‡] Nicolas Chevalier,[†] Denis Mariolle,[†] Denis Rouchon,[†] Hanako Okuno,[†,⊥] Vincent Bouchiat,[†,‖] and Gilles Cunge[†,‡]

[†]Université Grenoble Alpes, Grenoble F-38000, France
[‡]Laboratoire des Technologies de la Microélectronique, CNRS, Grenoble F-38054, France
[§]Laboratoire de Physique des Plasmas, Ecole Polytechnique/ Université Pierre-et-Marie-Curie/ Université Paris Sud-11/ CNRS, Palaiseau F-91128, France
[⊥]Institut Nanosciences et Cryogénie, CNRS, Grenoble F-38054, France
[‖]Institut Néel, Université Joseph-Fourier/ CNRS, Grenoble F-38042, France

[*]fdjawhar@uci.edu

ABSTRACT

The impact on the electronic and structural properties of CVD graphene transferred onto SiO_2/Si of continuous H_2-based plasmas, used to remove sticky residues composed of PMMA and Si-based nanoparticles at the surface, was investigated. By combining X-ray photoelectron spectroscopy (XPS) and Atomic Force Microscopy (AFM), we found that H_2 plasma treatment, which allows simultaneous etching of Si-based nanoparticles and PMMA, causes fragmentation of CVD graphene layer into nanoplatelets and subsequent etching of the uncovered SiO_2/Si surface. We added CF_4 into the H_2 plasma to allow the selective etching of Si-based impurities while maintaining the quality and stability of the CVD graphene. The increase in sp^2/sp^3 ratio and decrease in Si-C bonds, evaluated from XPS analysis, reveals the removal of all residual contamination. AFM analysis confirms the efficient and selective etching of residues from the surface of graphene, which displays a microscopic corrugation due to the weak coupling with the SiO_2/Si substrate. The established CF_4/H_2 plasma processing generates, however, cracks along grain boundaries in CVD graphene, which is responsible for unusual transport properties. Characterization of local chemical structures using Raman spectroscopy reveals that CVD graphene layer is essentially undamaged under the CF_4/H_2 plasma and the dehydrogenation is incomplete in the subsequent annealing at 400 °C. The local electronic structure is probed using reciprocal-space photoemission electron microscopy (k-PEEM) and reveals a small, negative shift below 0.1 eV of the Dirac point with respect to Fermi level, which is consistent with n-doping caused by trapped hydrogen species at the interface. Threshold photoemission electron microscopy (PEEM) analysis establishes the work function of CVD graphene to be 4.57 eV. This study reveals that the optimized cleaning process almost recovers the original properties of quasi-freestanding graphene.

Keywords: H_2-based plasma treatment; silicon and PMMA contamination; graphene cleaning; hydrogen intercalation; electronic and structural properties; photoelectron spectroscopy; Raman spectroscopy; photoemission electron microscopy.

I. Introduction

The emerging need for high-speed electronics and low energy consumption devices has motivated researchers to explore the potential applications of graphene and 2D materials due to their outstanding properties.[1–4] Furthermore, the controlled modification of their properties has a potential to complement or replace current materials toward task-specific application in catalysis, energy, and sensing.[5,6] These have led to extensive research efforts to synthesize large area, high-quality monolayer graphene.[7] For instance, the growth of graphene on various transition metal substrates via chemical vapor deposition (CVD) route is investigated. Much progress has been made for rigorous control over shape, size, and the uniformity of domains in polycrystalline graphene.[8,9] Recently, a millimeter to centimeter-sized graphene single crystals was achieved by modulating the nucleation site density on Cu substrates.[10–12] Moreover, tailoring the physical properties of CVD graphene for device applications requires more attention because it is sensitive to the influence of their immediate environment, including the supporting substrate, defects and surface contamination arising from the typical manufacturing process for fabricating 2D material devices. [13–15] The most known contaminants include poly (methylmethacrylate) (PMMA), used as a mechanical support to transfer CVD-grown graphene onto a target substrate or as a photolithographic mask for patterning, and Si-based nanoparticles impurities resulting from the CVD oven and the used-masks.[14,16,17]

A significant effort has been devoted to clean graphene while maintaining its high crystallinity and film quality.[16–23] Among such methods, plasma processing is considered as one of the most practical approaches for large-scale graphene treatment.[22,24,25] We recently reported the detailed mechanism of the H_2 plasma selective etching of sacrificial PMMA film on CVD-grown graphene on Cu.[17] In order to prevent graphene damage, the etching process has been accomplished by using plasma conditions in which the surface is bombarded by light and low energy ions (10 eV H_x^+ ions)[17]. Even if the H_2 plasma is shown to be efficient in removing the two types of residual PMMA, i.e. the amorphous $PMMA^A$ and the self-organized 2D structures $PMMA^G$, two reasons make it inconvenient to use. The H_2 plasma cleaning process leads to mobility and reorganization of Si-based nanoparticles impurities, which has been shown to slow down the lateral etching of $PMMA^G$, because Si atoms tend to accumulate at the edges of $PMMA^G$ flakes thus inhibiting their lateral etching by hydrogen radicals.[17] Furthermore, for high-performance device realization, it has been reported that H_2 plasma processing of graphene transferred onto the SiO_2 substrate may lead to the lift-off of the graphene layer.[16] This is due to the penetration of protons through graphene and their recombination that forms an H_2 gas between SiO_2 and graphene.[16] Meanwhile, it is shown that conditioning and cleaning the Al_2O_3 plasma reactor walls by a short SF_6 plasma treatment can remarkably improve the reproducibility of the surface processing by forming a stable AlF_3 thin layer on the reactor walls.[26] In fact, this plasma processing step, prior to any surface treatment, is required to prevent the release of highly reactive parasitic species such as O, which may affect the quality of graphene during processing.[26]

Here we present the impact of CF_4 addition in the H_2 inductively coupled plasma (ICP) cleaning processes, with a focus on the structural and electronic properties of polycrystalline CVD graphene film with few micron-size grains transferred onto SiO_2/Si substrate. Indeed, fluorocarbon plasmas have long

been known to be efficient for etching Si-based materials[27] and the motivation of adding CF_4 to H_2 is to clean simultaneously carbon-based and silicon-based residues from the graphene surface. To this end, we performed a comparative study of graphene surface modification during etching with H_2 and CF_4/H_2 continuous ICP plasmas. The cleaning efficiency and the properties of the plasma-treated CVD graphene are investigated using XPS, AFM, and Raman in conjunction with PEEM/ kPEEM. The impact of the plasma treatment on long-range electrical transport through CVD graphene is also discussed.

II. Cleaning of CVD graphene surfaces by H_2-based plasma: choice of plasma conditions

A simplified schematic that illustrates the transfer process at the origin of PMMA contamination as well as the cleaning process is presented in Figure 1. Basically, during PMMA solution-spinning, a uniform solid film of PMMA was formed after the evaporation of a solvent. Thermal treatment was employed to improve the adhesion of PMMA to graphene, which results in the reorganization of PMMA networks at the interface. Previous studies have shown three types of PMMA[17]; (1) thick layer of $PMMA^B$ associated to the disordered structure, (2) thin layer of $PMMA^A$ associated to disordered and dense structure at the interface and (3) thin layer of $PMMA^G$ associated to molecules, including PMMA and adsorbed solvent molecules, organized into 2D layers on graphene. Usually, after the transfer is completed, acetone is used to enable the etching of $PMMA^B$, while the plasma process is used for etching $PMMA^{A+G}$ and Si-based materials.

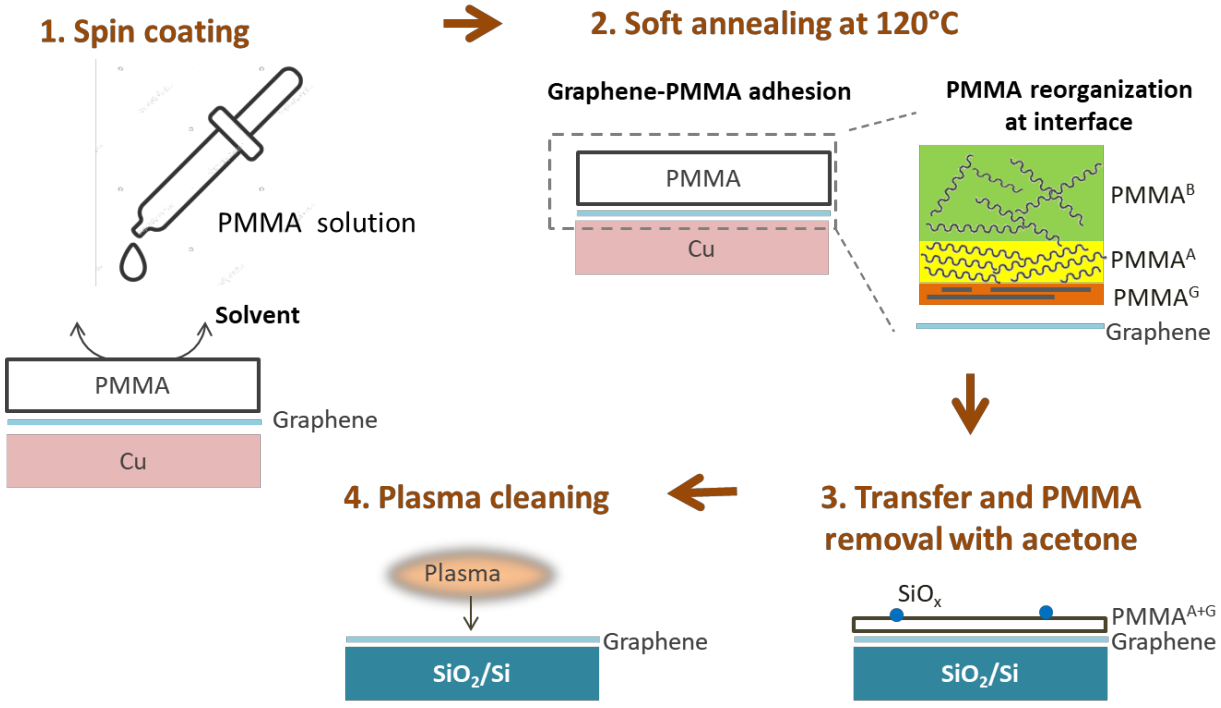

Figure 1: Schematic illustration of the CVD graphene transfer and cleaning processes.

To recover the electrical properties of the quasi-free-standing graphene layer, displaying zero band gaps and a band crossing at the Fermi level, an establishment of optimal plasma processing conditions is paramount. For this purpose, we have investigated the effect of three relevant plasma conditions in H_2 and CF_4/H_2 chemistry. The main challenge consists in eliminating the Si-based nanoparticles, which usually resists to hydrogen radicals and diffuses on graphene until they stick on edges of the $PMMA^G$ residues thus slowing down their elimination[17].

Typically, independent control of ion energy and plasma density can be provided by adjusting the source power. Thus, to achieve uniform high-density plasma and low-energy ions that ensure the appropriate surface cleaning of graphene, an intermediate ICP power of 800 W has been used. Here, we first report the effect of pure H_2 plasma. In order to achieve the reactive etching of Si-based material over graphene, we performed a comparative study between etching under conditions which are predominantly ion-assisted or radical-assisted. This is realized by varying the chamber pressure from 40 mT (condition 1) to 200 mTorr (condition 2), respectively. When the pressure is raised, the H atoms flux increases, while the H^+ ions fluxes and energy are significantly reduced. Therefore these conditions were chosen to analyze the respective roles of H atoms and ions on Si nanoparticles etching and graphene damages.

We also investigated the impact of CF_4/H_2 mixture plasma at high pressure, in which radical etching predominates over ion enhanced etching (condition 3). The idea here is simply that F atoms are known to be much more efficient than H to etch Silicon. The strategy is a two-step process: (i) a short step (10 s) in 0.5 % CF_4/H_2 plasma at 200 mTorr, used first to etch the silicon contamination, followed by (ii) a long step (80 s) in pure H_2 plasma at 200 mTorr to remove the remaining carbon-based contamination ($PMMA^{A+G}$). The optimal parameters, including CF_4 concentration and plasma exposure time, results from systematic XPS and optical microscopy investigations of the surface modification under several operating conditions. Our approach is based on the identification of conditions that allow the etching of Si-based material without damaging graphene by maintaining the exposure time to the CF_4/H_2 plasma shorter at lower CF_4 concentration that leads to (i) stable plasma and (ii) weak fluorine species diffusion through PMMA toward the graphene layer. Indeed, the chemisorption of fluorine results in strong out-of-plane corrugation of the graphene, which can make the structure more vulnerable to the hydrogen radicals[13,28]. It has been noticed that at higher CF_4 concentrations and longer exposure times, the plasma process generates defects in the graphene.

III. Effect of surface plasma treatment on the chemical composition and morphological properties

To assess the change in surface chemical composition of the CVD graphene transferred onto 5 nm-SiO_2/Si substrates after plasma etching of the residual contaminants, XPS investigations were performed. Figure 2 displays the C1s core level XPS spectra of (i) pre-treated CVD graphene, (ii) after H_2 plasma treatment for 20 s, 80 s and 140 s using 800 W source power at a working pressure of 40 mTorr (condition 1) and 200 mTorr (condition 2) and (iii) after CF_4–H_2 plasma treatment (condition 3). The

removal of chemisorbed H, which behaves like sp^3 defect (C-H bonds) in graphene lattice, was carried out via annealing in UHV at 400 °C. All spectra were normalized to Si2p component from the substrate.

Figure 2. a displays C1s spectrum from pre-treated CVD graphene/SiO_2/Si, which consists of four components from residual $PMMA^{A+G}$ located at 285.7 eV (C-H), 286.4 eV (C-C), 287.0 eV (C-O), and 288.9 eV (O-C=O), and two carbon hybridized components; sp^2 (C=C) at 284.4 eV from $PMMA^G$ and graphene and sp^3 (C-C) at 285.0 eV from $PMMA^G$ and defect structures in graphene.[17] An additional C1s component that is found at 283.9 eV is essentially attributed to the Si–C bonds present in the contamination[17]. This component was used as an indicator to (1) identify the graphene-like structure of $PMMA^G$ layers, decorated at edge sites by residual Si atoms, and (2) monitor the variations in Si-C bonds concentration arising from plasma interaction with Si-based nanoparticles enabling their diffusion or their etching. In this study, we do not present the Si2p spectra because contamination components overlap with those of the SiO_2/Si substrate. For line shape analysis, Voigt line shapes were used to fit components, whereas modified Doniach-Sunjic line shape (with a = 0.068 and g = 170 meV) was used to fit sp^2 component with a Shirley background subtraction. The sp^2 peak displays full width at half maximum (FWHM) of 0.71 eV which appears to be higher than what was of the high-quality CVD graphene grown on Cu displaying FWHM of about 0.45 eV, as can be seen in Figures S1 in the Supporting Information. Thus, the presence of $PMMA^{A+G}$ residues, in addition to constraint-based wrinkles, which arises from the transfer process of graphene[29], could be the origins for the increase of FWHM.

Figure 2. b displays C1s spectra from CVD graphene treated by low pressure H_2 plasma (condition 1), in which the representing surface is subjected to a high flux of relatively low energy (about 10 eV) hydrogen ions. This ion bombardment is required to etch the Si-based nanoparticle contamination. We first notice a decrease in the PMMA components intensity after 20 s of plasma treatment. At this stage, we assume that the plasma did not interact with graphene because it is still covered by a thin layer of $PMMA^G$. Although the reactive ion etching shows a decrease in $PMMA^G$ and Si-C bonds when the process duration is extended to 80 s, the graphene starts to be seriously damaged. This is evidenced by the large decay of the overall C1s intensity by a factor of 5, an increase in relative contribution of the sp^3 and the formation of C-O groups, found at 287.2 eV. If the process is further prolonged to 140 s, the C1s signal is now divided by 10, the sp^3/sp^2 intensity ratio increases dramatically (53 % contribution of sp^2) and we notice, in addition to CO, the presence of C-OH groups, seen at a binding energy of 285.8 eV, arising from oxygen atoms occupying the defects and edge sites in graphene. This indicates a severe degradation of the graphene structure by the plasma: after 140 s only flakes of graphene decorated by H and O remains. The exact mechanism whereby the graphene transferred onto the oxide substrate is damaged is yet to be elucidated. The ion energy is already high enough for protons to pass through graphene, but does not allow for the strong sp^2 bond breaking, as has been demonstrated previously for CVD graphene on Cu[17]. Thus, it is possible to consider (i) the presence of O species, originating from the reduction of the SiO_2 substrate underneath graphene, that contribute to graphene etching and/or (ii) the partial *lift-off* of the graphene or the formation of H_2 bubbles which leads to graphene cracks, as discussed in a recent paper[26]. Therefore, even if this plasma is able to remove $PMMA^G$ and related-silicon contaminations (after 140 s plasma exposure, the Si-C components becomes almost invisible), it cannot be use to clean graphene.

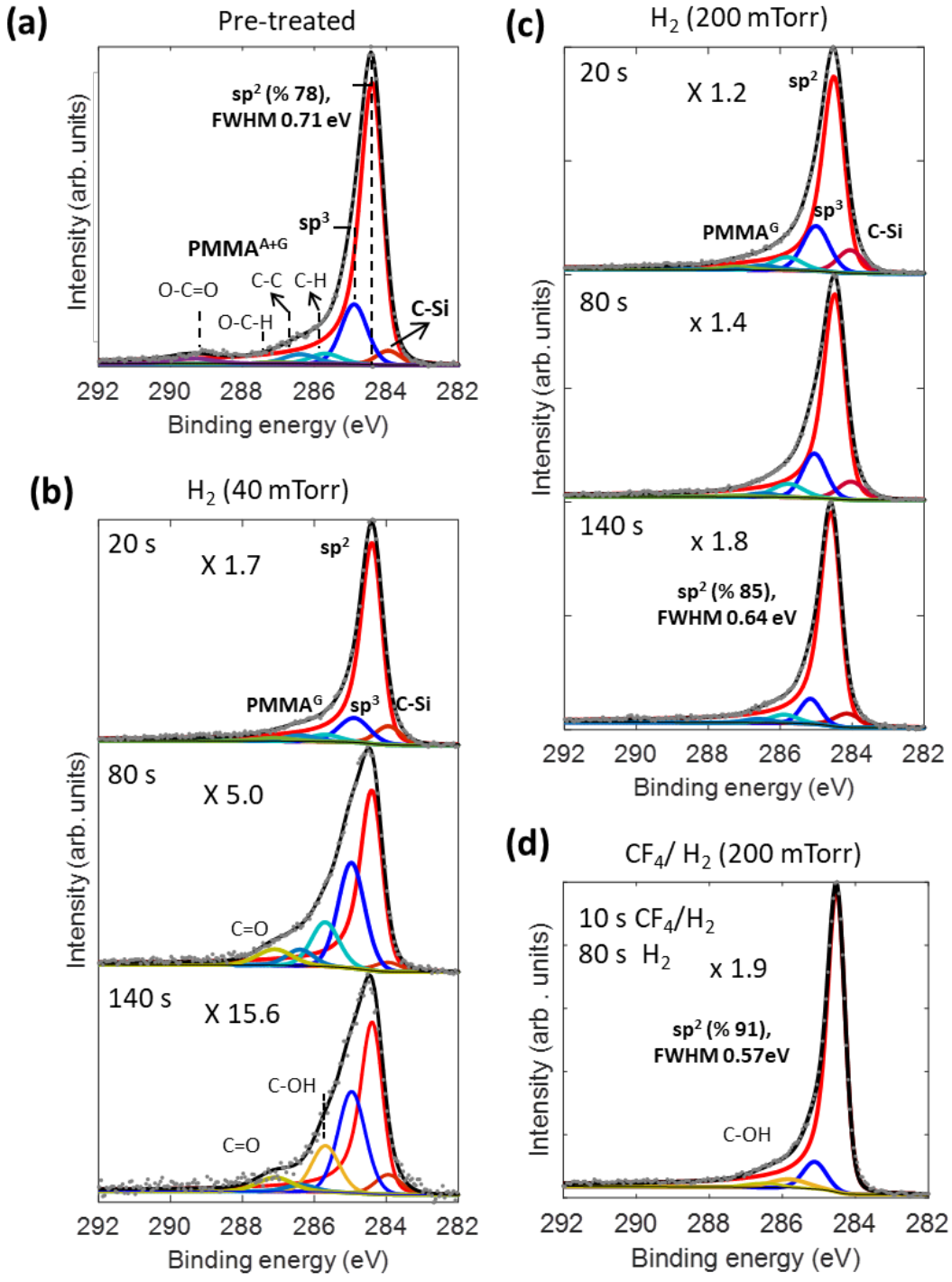

Figure 2: C1s core level spectra recorded before and after H_2-based plasma treatment of the CVD graphene transferred onto 5 nm-SiO_2/Si substrates at an ICP power of 800W: (a) pre-treated, (b) H_2 plasma at 40 mTorr for exposure time of 20s, 80s and 140s (c) H_2 plasma at 200 mTorr for exposure time of 20s, 80s and 140s and (d) CF_4/ H_2 plasma at 200 mTorr.

By contrast, the C1s spectra, shown in Figure 2. c, report the surface evolution under H_2 plasma working at condition 2, related mainly to the hydrogen radical etching. A statistical approach of the plasma phenomena suggests that reducing the ion-energy flux should significantly reduce the probability of graphene degradation. The relative intensity variation reveals a decrease in the PMMA, Si-C, and sp^3 components contribution as a function of plasma duration. The shape of C1s spectra remains unchanged after 140 s while the Si-C component is still present indicating incomplete cleaning of Si-related contamination, namely $PMMA^G$ and Si-based nanoparticles. This result indicates that CVD graphene processed with hydrogen radicals, did not suffer from damage and showed a higher intensity contribution of sp^2 (85 %) with a full width at half maximum (FWHM) of about 0.64 eV. The assessed FWHM of the sp^2 component is consistent with the presence of residual $PMMA^G$, which cannot be fully eliminated by H radicals alone in the presence of parasitic silicon residues.

Finally, Figure 2. d presents C1s spectrum obtained after plasma etching of $PMMA^G$ and Si using CF_4 and H_2 gases under condition 3. The deconvolution analysis indicates an sp^2 intensity contribution of 91 %, which is higher than those previously reported, with a full width at half maximum (FWHM) of about 0.54 eV, close to result obtained on as prepared CVD graphene layer on Cu foil. In addition, the Si-C component is not observed indicating the effectiveness of the plasma process to remove both the $PMMA^G$ and Si contamination. At this stage of the investigation, the exact origin of remnant sp^3 and C-OH components, associated to random defects in graphene, is unknown. To complement these observations, the surface morphology changes with aforementioned hydrogen-based plasma treatments are now examined.

Figure 3 shows AFM images (5 x 5 μm^2) and the corresponding surface roughness profiles, taken along the indicated lines, of aforementioned CVD graphene after the final plasma treatment under the condition 1, condition 2, and condition 3. AM-KPFM (Kelvin Probe Force Microscopy) images of untreated CVD graphene transferred onto 5 nm-SiO_2/Si showing PMMA and Si-based nanoparticle residual contamination are presented in Supporting Information S2. From all three of the aforementioned conditions, it is assumed that only $PMMA^G$ and Si-based contamination may be left on the surface. Identifying the remaining Si-based contamination with AFM and KPFM is challenging because the initial morphology of nanoparticles is not maintained under H_2 plasma (they diffuse on the surface)[17]; while the remaining 2D layers of $PMMA^G$ are expected to show an inter-plane distance similar to that of graphite. Figure 3. a displays the surface topography, obtained after plasma treatment under condition 1, and shows very rough structure, similar to the assembly of graphene nanoplatelets with an average diameter of 6 nm, which is well evidenced in the enlarged AFM image (1 x 1 μm^2). Although an efficient removal of $PMMA^G$ is achieved, this result shows that the graphene layer is fragmented by the plasma, caused by the creation of the defects in graphene and its subsequent lateral etching, in good agreement with previous XPS analysis. We also noticed a formation of 2 nm deep pores, which is associated to plasma etching of uncovered SiO_2/Si substrate.

The surface topography, obtained after plasma treatment under condition 2, is shown in Figure 3. b. This indicates a fairly homogeneous surface. The measured roughness corresponds to the 1-2 interlayer distance in graphite of 0.35 nm which can be explained by the heterogeneous coverage of graphene surface with 2D-like $PMMA^G$ layers of hundred-nanometer diameter, having an organizational structure

similar to that of graphene, as reported in previous paper[17]. This result indicates that the complete etching of PMMA[G] is not possible using H_2 plasma that does not damage graphene, which is in good agreement with previous statement derived from XPS results.

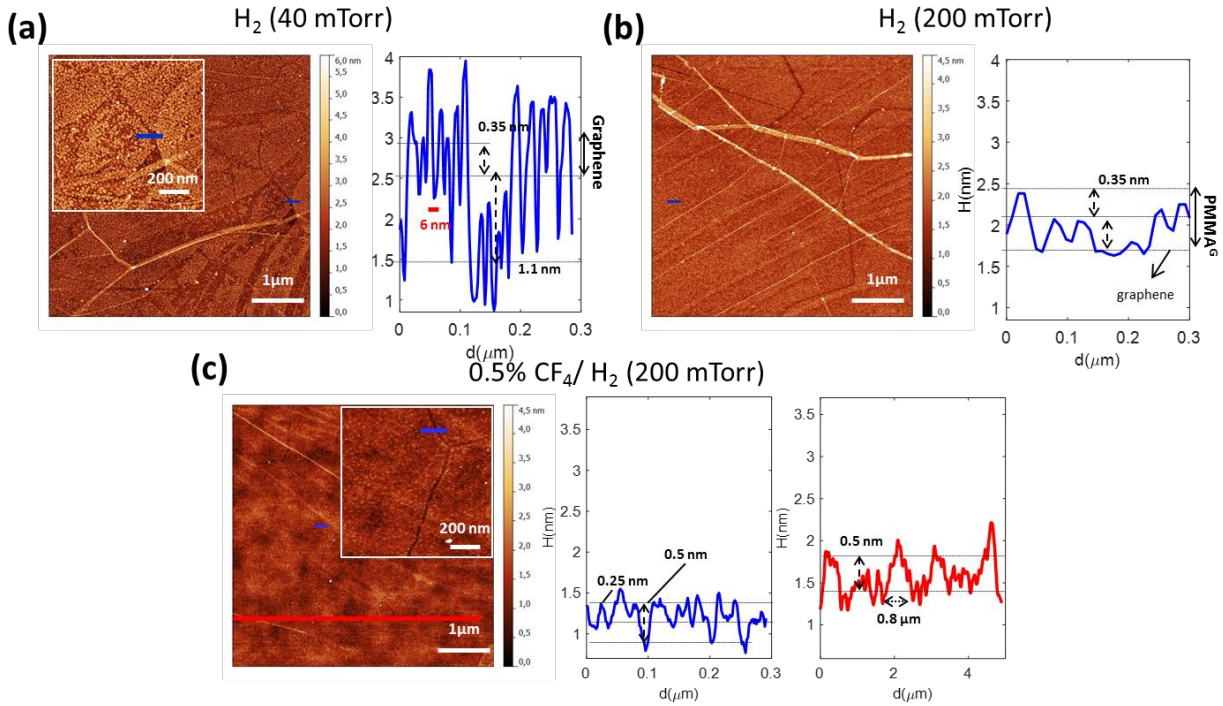

Figure 3: AFM images and the corresponding height profiles, taken along the indicated lines, of CVD graphene transferred onto 5 nm-SiO_2/Si substrate after plasma cleaning process (a) H_2 plasma at 40 mTorr (b) H_2 plasma at 200 mTorr and (c) optimized 0.5% CF_4/ H_2 plasma.

The surface topography, obtained after plasma treatment under condition 3, is seen in Figure 3. c. A nearly flat surface is observed. A short range roughness with an average amplitude of 0.25 nm (blue line profile), significantly lower than the interatomic distance in graphite, is observed. Since the XPS study indicates a good chemical structure of treated CVD graphene, the possible sources of this corrugation could be (i) a rough SiO_2/Si substrate surface[23], (ii) hydrogen passivation of SiO_2 surface and (iii) trapped hydrogen-based species at the surface that not completely desorb with thermal annealing treatment at 400 °C. We also identified the grains in CVD graphene layer having an average size of several microns, dissociating from each other at the grain boundaries. AFM topography image at a smaller field of view (1 x 1 µm^2) shows a maximum distance between two gains of 25 nm. Thus, the important height change seen is attributed to the plasma etching along grain boundaries of CVD graphene (strongly disordered area and particularly vulnerable to plasma processes) followed by the SiO_2/Si substrate etching. Therefore, the origin of small contribution of sp^3 and OH components, seen in C1s, is attributed to grain boundary/edge defects and plausible trap species at the interface. A long-range undulation (red line profile) with 0.5 nm out-of-plane deformation is clearly observed and associated to ripples in graphene with nearly quasi-free-standing behavior[30,31] due to low interaction with SiO_2/Si substrate. This may also explain the reduction of wrinkles from substrate constraint. Usually, the AFM analysis at this stage of

surface cleaning is difficult to obtain because of electrostatic interactions of graphene with the tip and weak coupling of graphene layer with the SiO_2/Si substrate. Basically, these results indicate that the surface cleaning of single crystal graphene, a sp^2-bonded carbon area, is effective using a mixture of CF_4/H_2 while maintaining its quality, in contrast to processing based on pure H_2 plasma, where the $PMMA^G$ layers resist to etching.

Although this treatment is efficient on single crystal graphene, the discontinuity at the grain boundaries in CVD graphene layer leads to unusual electrical transport measurements, as reported in Supporting Information S3. Indeed, the measurement of the resistivity as a function of the back gate voltage (V_{BG}) shows a charge neutrality point above 50 V and an increase in resistivity suggesting that treated-CVD graphene layer is heavily hole-doped and behaves like an insulator. In order to assess the effect of the established CF_4/H_2 plasma treatment on the local structural and electronic properties of plasma-treated CVD graphene, Raman and PEEM analysis are realized and described in the next section.

IV. Structural and electronic properties of optimized plasma-treated CVD graphene: defect and doping

To probe the impact of optimized-plasma processing on the structure of CVD graphene, Raman analysis has been performed using a laser at an excitation wavelength of 532 nm. Here, 300 nm-SiO_2/Si substrates are used to support CVD graphene because Raman signals, obtained from CVD graphene transferred onto 5 nm-SiO_2/Si substrates, are essentially weak. Previous XPS and AFM studies have addressed the plasma-induced irreversible defects in graphene; the systematic annealing after plasma treatment was carried out to desorb hydrogen from the surface and thus prevent a complication in the interpretation of the results. In this section, the surface characterization by Raman spectroscopy is reported before and after annealing in order to assess (i) the localization of adsorbed hydrogen and (ii) the doping level in graphene. Figure 4 shows four Raman spectra, consisting on the average measurements taken at a different position, of CVD graphene (i) without any treatment, (ii) after optimized plasma treatment and (iii) after optimized plasma and thermal annealing treatment.

Raman spectrum of untreated CVD graphene, shown in Figure 4. a, displays two typical peaks, G band ~ 1592 cm^{-1} and 2D band ~2695 cm^{-1}, involving phonons near the *K*-point at the Brillouin zone. The 2D mode decomposition in one component and G and 2D bands bandwidths of 13 and 35 cm^{-1}, respectively, indicate that analyzed areas are typically monolayer graphene. The defect-induced D band ~ 1354 cm^{-1}, arising when the translational symmetry of graphene is broken, is barely seen; a trivial contribution is mainly given by defects at grain boundaries in the CVD graphene[13]. Figure 4. b displays two spectra acquired at different positions, and obtained after plasma processing; these exhibit a different intensity of defect peaks. The D band intensity dependence with position indicates inhomogeneous distribution from plasma processing with localized areas displaying significant defect density. The intensity ratio of D and G peaks (A_D/A_G), about 0.6 to 1, suggests low to moderate defect density[13]. Another defect band, D', merge at 1620 cm^{-1}, indicating phonon confinement effect on the sp^2 region[32–34]. The appearance of this band reveals the formation of structural disorder that has an average defect separation on the order of a few nanometers.

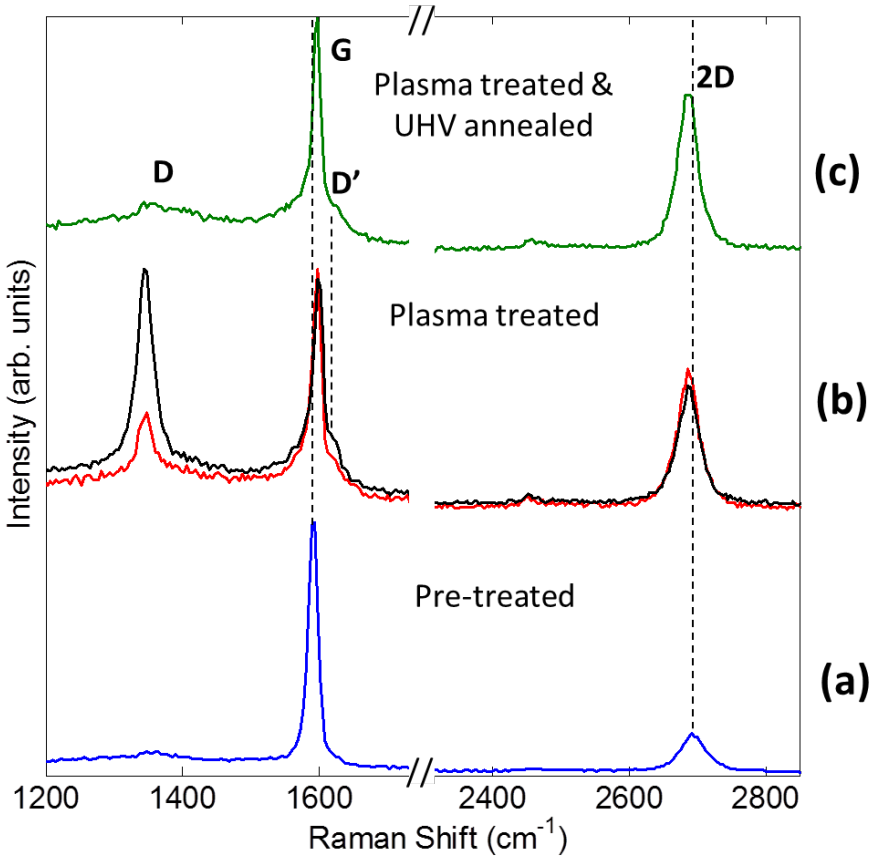

Figure 4: Raman spectra of CVD graphene transferred onto 300 nm-SiO_2/Si before and after surface processing. (a) Pre-treated, (b) plasma treated and (c) plasma treated and annealed.

Plasma-induced defect peaks may merge from irreversible vacancy defects or reversible sp^3-defects, induced by hydrogenation, through thermal annealing.[13,33] Based on literature[35–38], the variation in G and 2D peaks frequency depend on doping type; unlike the blue shift in the G peak, the blue-shift with p-doping and the red-shift with n-doping are reported in 2D peak. After plasma processing, we notice that G peak was shifted toward higher wavenumber by 6 cm^{-1} (blue shift), whereas 2D peak was shifted toward lower wavenumber by 8 cm^{-1} (red shift) revealing n-doping effect. The impact of residual PMMA-induced p-doping, acting as an electron acceptor, on the peak positions of the G and 2D have been studied, which reveals a weak blue-shifted of 1-4 cm^{-1} order of magnitude[39,40]. Thus, the observed n-doping can be explained by effective removal of PMMA residue and hydrogen chemisorption-induced n-doping through electron delocalization as result of C=C bonds breaking and C-H bonds formation[33,41,42]. An increase in the intensity ratio of 2D to G peaks (A_{2D}/A_G), which depends on the carrier density in graphene[37], is revealed. This observation confirms that the PMMA residues inducing p-doping are effectively removed. The annealing at 400 °C, performed to recover the undoped graphene surface, seems to boost more the intensity ratio A_{2D}/A_G, indicating that hydrogen adsorbates on graphene are removed, as reported in Figure 4. c. Although a considerable decrease in D intensity peak with annealing, associated to suppression of sp^3 –type defects in hydrogenated graphene[33,34,43], is shown, the

initial surface is not totally recovered. The remaining contribution is associated to trapped species at the interface and incomplete dehydrogenation which is supported by the unchanged 2D and G peaks position (n-doping). An annealing at a higher temperature may improve dehydrogenation processing but may also induce irreversible defects in graphene[23,44]. Unusually, a weak background ~1200-1600 cm^{-1} overlapping G and D' bands appears after plasma treatment which is consistent before and after annealing CVD graphene. Based on literature[44], this may be associated to undesorbed fragments of decomposed PMMA chains. These results are in agreement with the aforementioned XPS and AFM analysis, indicating that optimized plasma processing does not affect the graphene quality.

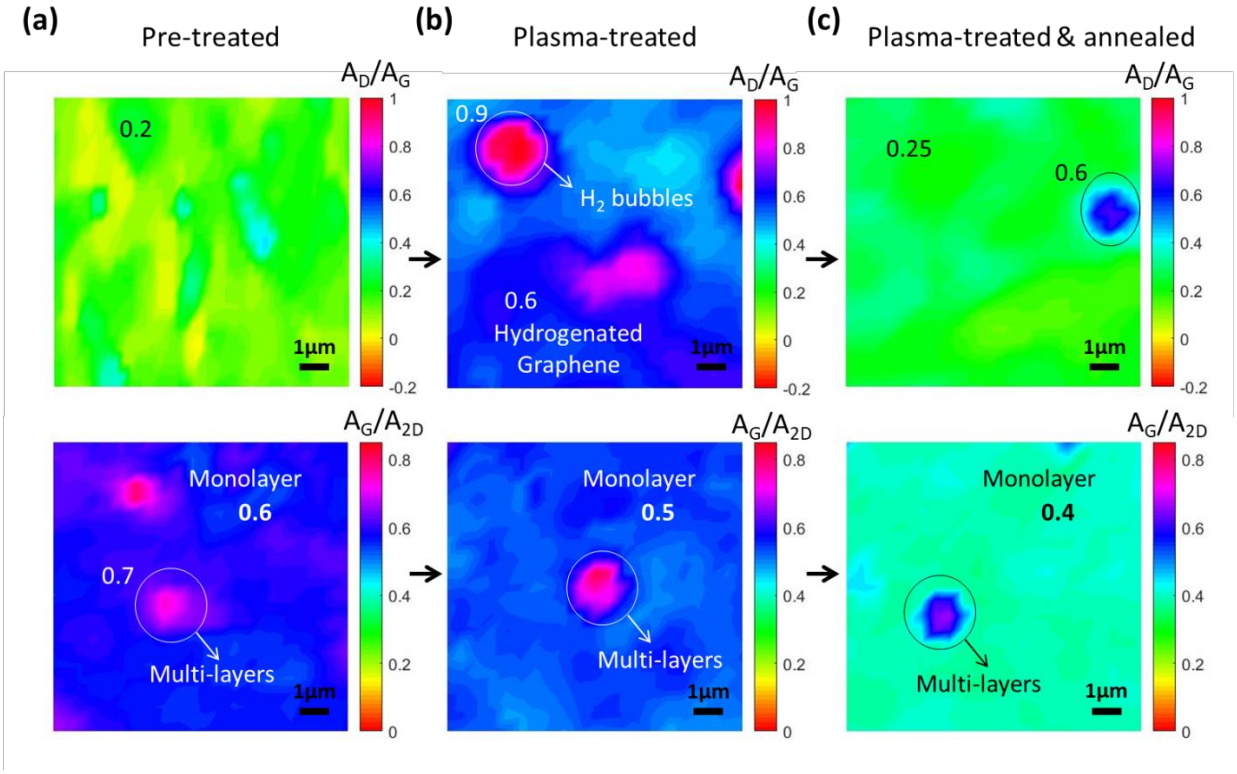

Figure 5: Intensity ratio maps of D to G band (A_D/A_G) and G to 2D band (A_G/A_{2D}) of CVD graphene transferred on 300 nm-SiO_2/Si: (a) as prepared, (b) plasma treated and (c) plasma treated and annealed.

In order to further demonstrate the effect of plasma and annealing treatment, intensity ratio maps of A_D/A_G and A_G/A_{2D} are reported in Figure 5. The measurements were taken from a (10 x 10 μm^2) area with a lateral resolution of 1 μm^2. Before treatment, A_D/A_G map, displayed in Figure 5 .a, basically reveals a weak and homogeneous spatial defect contribution. With A_G/A_{2D} map, seen in Figure 5 .a, we identify regions of multi-layer graphene, displaying higher intensity ratio of G to 2D bands. After plasma treatment, the A_D/A_G map, reported in Figure 5. b, shows an increase of defect intensity over the entire surface, displaying mainly two types of regions with moderate and low defect density. Most moderate defect density-regions have a circular shape of 1-2 µm diameter, suggesting the formation of hydrogen bubbles at the interface between the CVD graphene layer and the SiO_2/Si substrate. By observing A_D/A_G and A_G/A_{2D} maps, we found that hydrogenation coverage is independent on the number of layers. In principle, graphene exposed to H atoms only should not undergo a hydrogenation because it is

protected from chemisorption and penetration by the potential barrier originated from the π-electron cloud at sp^2-hybridized crystal structure[17,45]. However, hydrogenation happens because the CVD graphene surface is corrugated rather than flat, which significantly reduces the energy barrier. Furthermore, even if the ion energy and flux are significantly reduced at high pressure, the graphene remain bombarded by a low flux of H_x^+ ions with a high enough energy to chemisorb. After annealing, A_D/A_G and A_G/A_{2D} maps, seen in Figure 5. c, show values close to that of the reference sample, explained by a decrease in the total density of defects formed from hydrogenation, but not a complete disappearance (that may induce a slight n-doping). Basically, these results indicate that the optimized plasma-induced defect is a reversible process and can be recovered by annealing.

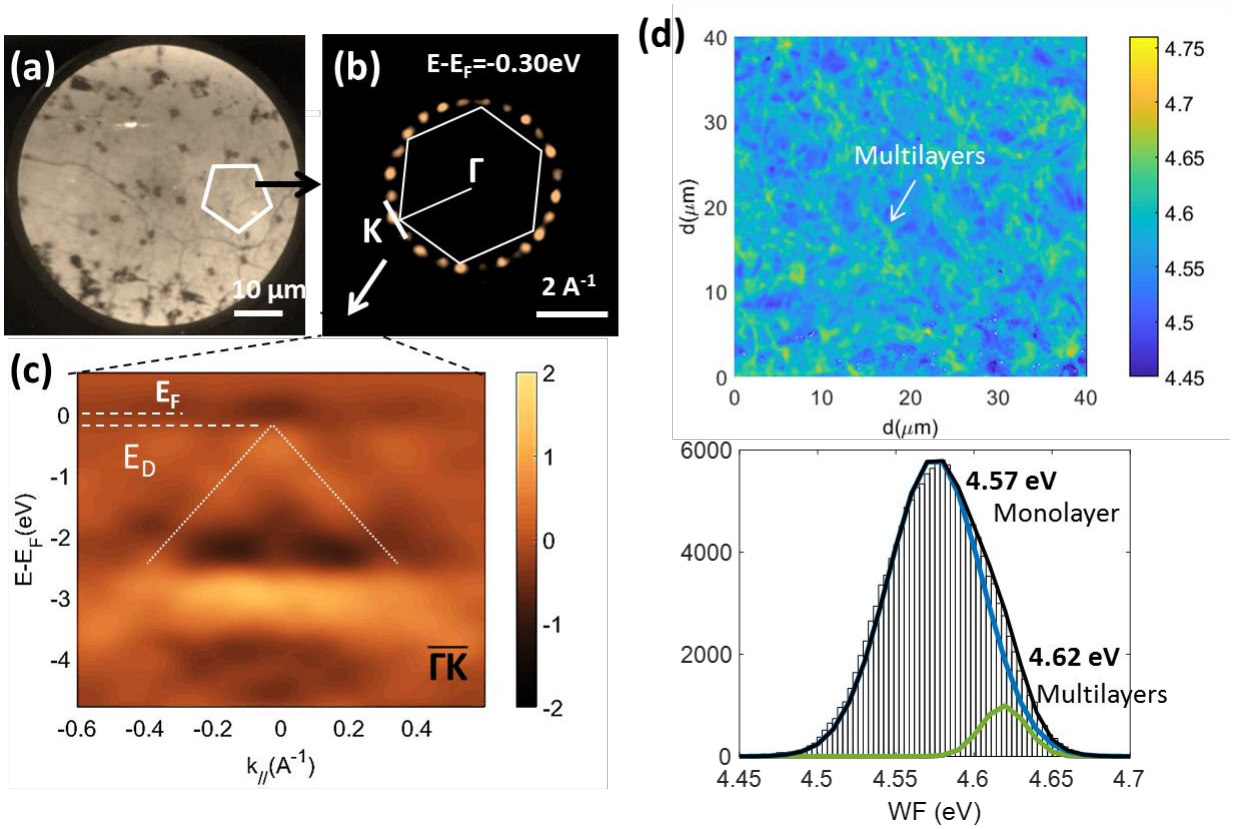

Figure 6: Plasma treated and annealed-CVD graphene transferred onto 5 nm-SiO_2/Si: (a) energy filtered PEEM image of 63 mm FoV acquired at a threshold energy (E-E_F =4.6 eV), (b) energy filtered k-PEEM image of a 5.1 $A^{\circ -1}$ FoV acquired at E-E_F =0.3 eV from 10 µm^2 selected area and (c) corresponding band structure along the $\overline{\Gamma K}$ direction showing a Dirac point shift with respect to Fermi level by 0.1 eV. (d) Work function map (42 x 42 µm^2) derived from the threshold PEEM analysis with the corresponding histogram.

2D-band structure imaging of individual single-crystal domain in CVD graphene, transferred onto 5 nm-SiO_2/Si substrate, after surface treatment is performed using momentum-resolved photoemission electron microscopy (k-PEEM) in UHV. Figure 6. a shows an energy filtered PEEM image (direct space, 63 µm FoV) acquired near threshold (E-E_F =4.6 eV), and showing mainly monolayer graphene with random

small multilayer (dark contrast). Figure 6. b shows an energy filtered kPEEM image (5.1 A^{-1} FoV) acquired close to the Fermi level ($E-E_F$ =0.3 eV) from a 10 µm selected area, which displays only monolayer graphene, shown in Figure 6. a. The obtained k-PEEM patterns show a set of six-fold symmetry photoemission spots related to the Dirac cones from grains in the CVD graphene. These are rotated relative to each other by approximatively 30 °, indicative of multiple domains rotated in-plane within the selected region. The corresponding band structure along the $\overline{\Gamma K}$ direction, characteristic of one domain, is displayed in Figure 6. c. A negative energy shift of ~ 0.1 eV of Dirac point with respect to the Fermi level is revealed, suggesting n-doping in agreement with Raman observations. The Dirac cone is close to the Fermi level; the complete desorption of hydrogen by annealing may lead to zero intrinsic doping and therefore the Fermi level at Dirac point.

Figure 6. d shows the work function map (42 x 42 μm^2) and corresponding histogram, recorded on the aforementioned sample. This map indicates a homogenous surface with an average work function value of 4.57 ± 0.2 eV for graphene monolayer, which is very close to that evaluated for multilayers areas of 4.62± 0.2 eV. The assessed value is in good agreement with that established in literature for un-doped single-layer graphene[46–48], where the Fermi level falls in the Dirac point. However, some other studies report a lower value of 4.2-4.3 eV for single layer graphene supported on SiC or SiO_2/Si substrates[49,50], which most likely forms Schottky junction at the interface with p-type charge transfer doping, or have adsorbates at surface[48,51]. Thus, the weak coupling between the graphene layer and SiO_2/Si substrate, as suggested by AFM observations, and lack of surface doping, evidenced by a k-PEEM study showing a tiny change in graphene Fermi level E_F, may explain the obtained work function value. Indeed, the shift of the Fermi level due to doping-induced charge carrier density modulation mostly impacts the graphene work function; it essentially increases with the electron-doping and decreases with the hole –doping[52–54]. A notable impact of residual trapped H species, seen to increase slightly charge carriers, is not discerned, while moderate coverage of hydrogen can yield a larger work function change[33,41,55]. The presence of discontinuous coverage of $PMMA^G$ on graphene induced-hole doping shows a small increase in work function, evaluated to 4.65 eV. The corresponding work function map is included in the Supporting Information S4. The recovering of expected graphene work function with optimized plasma treatment, confirms the effectiveness of the process for removal of PMMA and Si contamination. Furthermore, the low-pressure ions-based H_2 plasma treatment dramatically lowers the work function from 4.65 eV, in presence of $PMMA^G$, down to 3.5 eV as a result of the introduction of vacancy-based defects in graphene, as reported in Supporting Information S4. Therefore, modulation and tuning of H_2-based plasma conditions is crucial for improving surface graphene cleaning.

Conclusion

The transfer process of CVD graphene grown on Cu foil to other substrates usually generates two types of contamination: PMMA and Si nanoparticles. A cleaning method based on H_2 plasma treatment in combination with annealing at 400 °C in UHV yields the removal of most of the residual polymer but is not able to fully etch Si-based contamination, including $PMMA^G$ layers, without damaging graphene structure. The surface cleaning, obtained by CF_4/ H_2 radical etching, eventually results in the effective removal of the Si-based nanoparticles and residual PMMA. Although plasma does not affect the

properties of the sp^2 structure, at the grain boundary the formation of cracks of a few nanometers length is observed because of typical weak binding (vulnerable region). This results in unusual electronic properties displaying such heavily p-doped and resistive CVD graphene layer while the local electronic structure investigation reveals graphene that is somewhat n-doped by residual adsorbed hydrogen, displaying ~ 0.1 eV shift in the Dirac point. Although our investigation shows that the optimized plasma treatment almost restores the original electronic properties of single crystal and un-doped graphene layer, improvement in the cleaning process is needed. Ideal conditions are a high flux of thermal H and F atoms without ions and at high temperatures (PMMA etching is thermally assisted). This could be achieved in downstream plasma thus reducing the amount of hydrogen adsorbed and H trapped underneath graphene, and perhaps avoid the grain boundaries deterioration in CVD graphene.

Experimental

The plasma etching is carried out in an industrial high-density ICP source (DPS AdvantEdge^{TM}) from Applied Materials design to etch 300 mm diameter wafers[56]. To prevent the presence of contamination deposited during the etching process and parasitic O in the plasma due to Al_2O_3 reactor wall corrosion in reactive H_2 plasma, the plasma reactor wall is cleaned and coated with a resistive ALF_3 layer using typical industrial cleaning process with a SF_6/O_2 plasma[57] and conditioning NF_3 plasma in between each experiment. For the same reason, we use 300 mm diameter wafer holders made of fluorinated Al_2O_3 (AlF_3@Al_2O_3 thin layer on a silicon wafer) to introduce and hold small graphene samples in the reactor. The effect of plasma and reactor wall coating on the treatment of fragile 2D material has been detailed on another paper[26]. Samples are stuck with kaptonTM tape on the wafer, and the temperature is kept at 65^{o} C with a He backside cooling. The ICP in a continuous (CW) mode has been used to process the graphene samples.

Samples used in this study are commercially produced large area CVD graphene monolayer from Graphenea Company. We use two different types of graphene samples: PMMA-assisted CVD graphene transfer onto SiO_2 (300 nm thick)/Si and Si (with native SiO_2) substrates. The sacrificial thin layer of PMMA (400 nm), used for transfer processing, is removed with acetone.

The **XPS** measurements over an area of few mm^2 were carried out at a base pressure 10^{-9} mbar in a Multiprobe spectrometer (ScientaOmicron) equipped with a monochromatized Al Kα source (1486.6 eV) and a 128 channel, parallel detection Argus electron analyzer. The overall energy resolution was 270 meV. The emission angle is fixed to 20° with respect to the surface normal. Thus, the probed depth is about 8 nm for PMMA and graphene (λ~3nm). The spectrometer chamber is connected to a preparation chamber in which samples could be annealed in ultrahigh vacuum (10^{-9} mbar) in order to remove chemisorbed plasma species and impurities.

The **X-PEEM and k-PEEM** experiments were performed in an ultra-high vacuum chamber using a NanoESCA spectromicroscope (ScientaOmicron), described previously elsewhere[58]. The spectromicroscope is equipped with three different monochromatized sources, Al Kα (1486.6 eV), He II (21.2) and Hg (4.9 eV). A double pass hemispherical energy analyzer was used to compensate single analyzer aberrations imaging. A 68 µm field of view was used with 12 kV extraction voltage and about

1.8 mm sample-objective lens distance. The overall energy resolution of the analysis was 200 meV (Pass Energy of 50 eV, slit 1). A contrast aperture of 500 µm was used corresponding to a lateral resolution of about 0.5 µm. The energy filtered PEEM image series was acquired at the photoemission threshold region using He II source and in the C1s, Si2p region using X-ray source. After correction for the Schottky effect of 98 meV because of the high extractor field, the fit of the photoemission threshold spectra with error function can be used to directly measure the local work function. Then, the series of images taken at an increasing photoelectron kinetic energy enables us to determine work function map obtained from the fit of the spectrum for each pixel. In the same way, the XPS spectra of a selected small area were acquired. The k-PEEM results were acquired using He II source and fully opened aperture 1500 µm. This was required to image a sufficient portion of reciprocal space in order to cover a full Brillouin zone. The area of interest on the sample surface is chosen by a field aperture situated in an intermediate image plane that was closed down to about 10 µm. A transfer lens then projected the 1500 µm diameter disk of the focal plane via the energy analyzer onto the detector giving a 2D k-space dimension of about ±2.5°A^{-1} around the point. The wave vector resolution is ~0.05°A^{-1}. The detector response was corrected by the flat field of the detector and camera defects were eliminated using dark images. With our graphene/SiO_2/Si samples, it was found out that additional sample illumination with UV light (4.9 eV) using a Hg arc lamp allows for stable measurement.

The **AFM** measurements were carried out in tapping mode on a Dimension Icon from Bruker. Standard silicon tips from Budget Sensors (TAP300Al-G) with a first resonant frequency of 300 kHz range and a nominal spring constant of 40 N/m were used. Areas of 1 x 1 μm^2 and 5 x 5 μm^2 with a 512 x 512 pixels resolution were typically analyzed.

The **µ-Raman** measurements were performed with a commercial Witec Alpha 500 spectrometer set-up with a dual-axis X-Y piezo stage. Dual Laser with 532 nm excitation wavelength was used with 0.1 mW power. The grating had 1,800 lines per mm in the best case, conferring a spectral resolution of 0.01 cm^{-1}. Raman spectra were recorded in the air with a Nikon x100 objective focusing the light on a 320 nm-diameter spot. Raman shifts are calibrated using the silicon line as a reference. Raman cartographies recorded on graphene samples were computed with the Labspec5 program.

Electron transport properties involved a Signal Recovery PAR Lock-in amplifier with a current bias detection using a 10 Mega Ohm bias resistor in series with the sample. The silicon sample is used as a back gate to measure the field effect of the graphene sheet.

Acknowledgments

The authors thank the French Research Agency through Clean-Graph project ANR-13-BS09-0019-04. The measurements were made on both the CEA Minatec Nanocharacterization Platform (PFNC) and the clean rooms of CEA-LETI.

Present Addresses

Djawhar Ferrah, Department of Chemistry, University of California, Irvine, CA 92697, United States

Author contributions

Gilles Cunge, Olivier Renault and Vincent Bouchiat were involved in planning and supervised the work and the findings. Gilles Cunge is specialized in the plasma-based material processing. Olivier Renault is specialized in the surface analysis and especially in the XPEEM/ KPEEM characterization technique. Vincent Bouchiat is specialized in synthesis of 2D material and their electrical characterization. Djawhar Ferrah and Gilles Cunge contributed to the implementation of the plasma processes. Djawhar Ferrah processed and subsequently characterized samples with XPS and PEEM spectroscopy helped by Olivier Renault. Nicolas Chevalier and Denis Mariolle performed the AFM measurements. Vincent Bouchiat and Daniil Marinov performed the Raman measurements and electrical measurements. Djawhar Ferrah processed the experimental data, performed the analysis, drafted the manuscript and designed the figures. Denis Rouchon helped in interpreting the Raman results and characterization (not reported here). Javier Arias-Zapata helped in sample preparation and SEM analysis (not reported here). All authors discussed the results and commented on the manuscript.

ASSOCIATED CONTENT

Supporting Information available: [C1s spectrum obtained from CVD graphene grown on Cu foil; AM-KPFM imaging of pre-treated CVD graphene transferred onto 5nm-SiO_2/Si; Electrical transport properties of optimized plasma-treated CVD graphene; Work function measurement on pure H_2 plasma-treated CVD graphene; Pressure tuning for plasma cleaning process optimization]

References

(1) Ferrari, A. C.; Bonaccorso, F. ; Fal'ko, V.; Novoselov, K. S.; Roche, S.; Bøggild, P.; Borini, S.; Koppens, F. H. L.; Palermo, V.; Pugno, N.; Garrido, J. A.; Sordan, R.; Bianco, A.; Ballerini, L.; Prato, M.; Lidorikis, E.; Kivioja, J.; Marinelli, C.; Ryhänen, T.; Morpurgo, A.; Coleman, J. N.; Nicolosi, V.; Colombo, L.; Fert, A.; Garcia-Hernandez, M.; Bachtold, A.; Schneider, G. F.; Guinea, F.; Dekker, C.; Barbone, M.; Sun, Z.; Galiotis, C.; Grigorenko, A. N.; Konstantatos, G.; Kis, A.; Katsnelson, M.; Vandersypen, L.; Loiseau, A.; Morandi, V.; Neumaier, D.; Treossi, E.; Pellegrini, V.; Polini, M.; Tredicucci, A.; Williams, G. M.; Hong, B. H.; Ahn, J-H; Kim, J. M.; Zirath, H.; Wees, B. J. V; Van Der Zant, H.; Occhipinti, L.; Di Matteo, A.; Kinloch, I. A.; Seyller, T.; Quesnel, E.; Feng, X.; Teo, K.; Rupesinghe, N.; Hakonen, P.; Neil, S. R. T.; Tannock, Q.; Löfwander, T.;Kinaret, J. Science and Technology Roadmap for Graphene, Related Two-Dimensional Crystals, and Hybrid Systems. *Nanoscale* **2015,** *7*, 4598-4810.

(2) Novoselov, K. S.; Fal'Ko, V. I.; Colombo, L.; Gellert, P. R.; Schwab, M. G.; Kim, K. A Roadmap for Graphene. *Nature*. **2012**, *490*, 192-200.

(3) Chen, Z.; Lin, Y. M.; Rooks, M. J.; Avouris, P. Graphene Nano-Ribbon Electronics. *Phys. E Low-Dimensional Syst. Nanostructures* **2007,** *40*, 228-232.

(4) Xia, F.; Farmer, D. B.; Lin, Y. M.; Avouris, P. Graphene Field-Effect Transistors with High on/off Current Ratio and Large Transport Band Gap at Room Temperature. *Nano Lett.* **2010**, *10*, 715-718.

(5) Georgakilas, V.; Tiwari, J. N.; Kemp, K. C.; Perman, J. A.; Bourlinos, A. B.; Kim, K. S.; Zboril, R. Noncovalent Functionalization of Graphene and Graphene Oxide for Energy Materials, Biosensing, Catalytic, and Biomedical Applications. *Chemical Reviews*. **2016**, *116*, 5464-5519.

(6) Tozzini, V.; Pellegrini, V. Prospects for Hydrogen Storage in Graphene. *Physical Chemistry Chemical Physics*. **2013**, *15*, 80-89.

(7) Choi, W.; Lahiri, I.; Seelaboyina, R.; Kang, Y. S. Synthesis of Graphene and Its Applications: A Review. *Crit. Rev. Solid State Mater. Sci.* **2010**, *35*, 52-71.

(8) Ma, T.; Ren, W.; Zhang, X.; Liu, Z.; Gao, Y.; Yin, L.-C.; Ma, X.-L.; Ding, F.; Cheng, H.-M. Edge-Controlled Growth and Kinetics of Single-Crystal Graphene Domains by Chemical Vapor Deposition. *Proc. Natl. Acad. Sci.* **2013,** *110*, 20386-20391.

(9) Murdock, A. T.; Koos, A.; Britton, T. Ben; Houben, L.; Batten, T.; Zhang, T.; Wilkinson, A. J.; Dunin-Borkowski, R. E.; Lekka, C. E.; Grobert, N. Controlling the Orientation, Edge Geometry, and Thickness of Chemical Vapor Deposition Graphene. *ACS Nano* **2013,** 7, 1351-1359.

(10) Wu, T.; Zhang, X.; Yuan, Q.; Xue, J.; Lu, G.; Liu, Z.; Wang, H.; Wang, H.; Ding, F.; Yu, Q.; Xie, X.; Jiang, M. Fast Growth of Inch-Sized Single-Crystalline Graphene from a Controlled Single Nucleus on Cu-Ni Alloys. *Nat. Mater.* **2016,** *15*, 43-47.

(11) Mohsin, A.; Liu, L.; Liu, P.; Deng, W.; Ivanov, I. N.; Li, G.; Dyck, O. E.; Duscher, G.; Dunlap, J. R.; Xiao, K.; Gu, G. Synthesis of Millimeter-Size Hexagon-Shaped Graphene Single Crystals on Resolidified Copper. *ACS Nano* **2013,** *7*, 8924-8931.

(12) Yan, Z.; Lin, J.; Peng, Z.; Sun, Z.; Zhu, Y.; Li, L.; Xiang, C.; Samuel, E. L.; Kittrell, C.; Tour, J. M. Toward the Synthesis of Wafer-Scale Single-Crystal Graphene on Copper Foils. *ACS Nano* **2012,** *6*, 9110-9117.

(13) Eckmann, A.; Felten, A.; Mishchenko, A.; Britnell, L.; Krupke, R.; Novoselov, K. S.; Casiraghi, C. Probing the Nature of Defects in Graphene by Raman Spectroscopy. *Nano Lett.* **2012**, *12*, 3925-3930.

(14) Pirkle, A.; Chan, J.; Venugopal, A.; Hinojos, D.; Magnuson, C. W.; McDonnell, S.; Colombo, L.; Vogel, E. M.; Ruoff, R. S.; Wallace, R. M. The Effect of Chemical Residues on the Physical and Electrical Properties of Chemical Vapor Deposited Graphene Transferred to SiO_2. *Appl. Phys. Lett.* **2011,** *99*, 122108.

(15) Zhou, S. Y.; Gweon, G. H.; Fedorov, A. V.; First, P. N.; De Heer, W. A.; Lee, D. H.; Guinea, F.; Castro Neto, A. H.; Lanzara, A. Substrate-Induced Bandgap Opening in Epitaxial Graphene. *Nat. Mater.* **2007,** *6*, 770-775.

(16) Ferrah, D.; Renault, O.; Petit-Etienne, C.; Okuno, H.; Berne, C.; Bouchiat, V.; Cunge, G. XPS Investigations of Graphene Surface Cleaning Using H_2- and Cl_2-Based Inductively Coupled Plasma. In *Surface and Interface Analysis*; **2016**, *48*, 451-455.

(17) Cunge, G.; Ferrah, D.; Petit-Etienne, C.; Davydova, A.; Okuno, H.; Kalita, D.; Bouchiat, V.; Renault, O. Dry Efficient Cleaning of Poly-Methyl-Methacrylate Residues from Graphene with High-Density H_2 and H_2-N_2 Plasmas. *J. Appl. Phys.* **2015**, *118*, 123302.

(18) Moser, J.; Barreiro, A.; Bachtold, A. Current-Induced Cleaning of Graphene. *Appl. Phys. Lett.* **2007**, *91*, 163513.

(19) Algara-Siller, G.; Lehtinen, O.; Turchanin, A.; Kaiser, U. Dry-Cleaning of Graphene. *Appl. Phys. Lett.* **2014**, *104*, 153115.

(20) Goossens, A. M.; Calado, V. E.; Barreiro, A.; Watanabe, K.; Taniguchi, T.; Vandersypen, L. M. K. Mechanical Cleaning of Graphene. *Appl. Phys. Lett.* **2012**, *104*, 153115.

(21) Lindvall, N.; Kalabukhov, A.; Yurgens, A. Cleaning Graphene Using Atomic Force Microscope. *J. Appl. Phys.* **2012**, *111*, 064904.

(22) Lim, Y. D.; Lee, D. Y.; Shen, T. Z.; Ra, C. H.; Choi, J. Y.; Yoo, W. J. Si-Compatible Cleaning Process for Graphene Using Low-Density Inductively Coupled Plasma. *ACS Nano* **2012**, *6*, 4410-4417.

(23) Cheng, Z.; Zhou, Q.; Wang, C.; Li, Q.; Wang, C.; Fang, Y. Toward Intrinsic Graphene Surfaces: A Systematic Study on Thermal Annealing and Wet-Chemical Treatment of SiO_2-Supported Graphene Devices. *Nano Lett.* **2011**, *11*, 767-771.

(24) Friedrich, J. F.; Hidde, G.; Lippitz, A.; Unger, W. E. S. Plasma Bromination of Graphene for Covalent Bonding of Organic Molecules. *Plasma Chemistry and Plasma Processing.* **2014**, *34*, 621-645.

(25) Lee, B. J.; Lee, B. J.; Lee, J.; Yang, J. W.; Kwon, K. H. Effects of Plasma Treatment on the Electrical Reliability of Multilayer MoS_2 field-Effect Transistors. *Thin Solid Films* **2017**, *637*, 32-36.

(26) Mehedi, H.-A.; Ferrah, D.; Dubois, J.; Petit-Etienne, C.; Okuno, H.; Bouchiat, V.; Renault, O.; Cunge, G. High Density H_2 and He Plasmas: Can They Be Used to Treat Graphene? *J. Appl. Phys.* **2018**, *124*, 125304.

(27) Mogab, C. J.; Adams, A. C.; Flamm, D. L. Plasma Etching of Si and SiO_2- The Effect of Oxygen Additions to CF_4 plasmas. *J. Appl. Phys.* **1978**, *49*, 3796-3803.

(28) Chronopoulos, D. D.; Bakandritsos, A.; Pykal, M.; Zbořil, R.; Otyepka, M. Chemistry, Properties, and Applications of Fluorographene. *Applied Materials Today*. **2017**, *9*, 60-70.

(29) Liu, N.; Pan, Z.; Fu, L.; Zhang, C.; Dai, B.; Liu, Z. The Origin of Wrinkles on Transferred Graphene. *Nano Res.* **2011**, *4*, 996-1004.

(30) Fasolino, A.; Los, J. H.; Katsnelson, M. I. Intrinsic Ripples in Graphene. *Nat. Mater.* **2007**, *6*, 858-861.

(31) Meyer, J. C.; Geim, A. K.; Katsnelson, M. I.; Novoselov, K. S.; Booth, T. J.; Roth, S. The Structure of Suspended Graphene Sheets. *Nature.* **2007**, *446*, 60-63.

(32) Martins Ferreira, E. H.; Moutinho, M. V. O.; Stavale, F.; Lucchese, M. M.; Capaz, R. B.; Achete, C. A.; Jorio, A. Evolution of the Raman Spectra from Single-, Few-, and Many-Layer Graphene with Increasing Disorder. *Phys. Rev. B.* **2010,** *82*, 125429.

(33) Luo, Z.; Yu, T.; Ni, Z.; Lim, S.; Hu, H.; Shang, J.; Liu, L.; Shen, Z.; Lin, J. Electronic Structures and Structural Evolution of Hydrogenated Graphene Probed by Raman Spectroscopy. *J. Phys. Chem. C.* **2011**, *115*, 1422-1427.

(34) Withers, F.; Russo, S.; Dubois, M.; Craciun, M. F. Tuning the Electronic Transport Properties of Graphene through Functionalisation with Fluorine. *Nanoscale Res. Lett.* **2011,** *6*, 526.

(35) Pisana, S.; Lazzeri, M.; Casiraghi, C.; Novoselov, K. S.; Geim, A. K.; Ferrari, A. C.; Mauri, F. Breakdown of the Adiabatic Born-Oppenheimer Approximation in Graphene. *Nat. Mater.* **2007**, *6*, 198-201.

(36) Yan, J.; Zhang, Y.; Kim, P.; Pinczuk, A. Electric Field Effect Tuning of Electron-Phonon Coupling in Graphene. *Phys. Rev. Lett.* **2007**, *98*, 166802.

(37) Das, A.; Pisana, S.; Chakraborty, B.; Piscanec, S.; Saha, S. K.; Waghmare, U. V.; Novoselov, K. S.; Krishnamurthy, H. R.; Geim, A. K.; Ferrari, A. C.; Sood, A. K. Monitoring Dopants by Raman Scattering in an Electrochemically Top-Gated Graphene Transistor. *Nat. Nanotechnol.* **2008,** *3*, 210-215.

(38) Casiraghi, C.; Pisana, S.; Novoselov, K. S.; Geim, A. K.; Ferrari, A. C. Raman Fingerprint of Charged Impurities in Graphene. *Appl. Phys. Lett.* **2007,** *91*, 233108.

(39) Kumar, K.; Kim, Y. S.; Yang, E. H. The Influence of Thermal Annealing to Remove Polymeric Residue on the Electronic Doping and Morphological Characteristics of Graphene. *Carbon N. Y.* **2013**, *65*, 35-45.

(40) Choi, W.; Shehzad, M. A.; Park, S.; Seo, Y. Influence of Removing PMMA Residues on Surface of CVD Graphene Using a Contact-Mode Atomic Force Microscope. *RSC Adv.* **2017**, *7*, 6943-6949.

(41) Matis, B. R.; Burgess, J. S.; Bulat, F. A.; Friedman, A. L.; Houston, B. H.; Baldwin, J. W. Surface Doping and Band Gap Tunability in Hydrogenated Graphene. *ACS Nano* **2012,** *6*, 17-22.

(42) Park, M.; Yun, Y. J.; Lee, M.; Jeong, D. H.; Jun, Y.; Park, Y. W.; Kim, B. H. Local Doping of Graphene Devices by Selective Hydrogen Adsorption. *AIP Adv.* **2015**, *5*, 017120.

(43) Elias, D. C.; Nair, R. R.; Mohiuddin, T. M. G.; Morozov, S. V.; Blake, P.; Halsall, M. P.; Ferrari, A. C.; Boukhvalov, D. W.; Katsnelson, M. I.; Geim, A. K.; Novoselov, K. S. Control of Graphene's Properties by Reversible Hydrogenation: Evidence for Graphane. *Science.* **2009**, *323*, 610-613.

(44) Gong, C.; Floresca, H. C.; Hinojos, D.; McDonnell, S.; Qin, X.; Hao, Y.; Jandhyala, S.; Mordi, G.; Kim, J.; Colombo, L.; Ruoff, R. S.; Kim, M. J.; Cho, K.; Wallace, R. M.; Chabal, Y. J. Rapid Selective Etching of PMMA Residues from Transferred Graphene by Carbon Dioxide. *J. Phys. Chem. C* **2013**, *117*, 23000-23008.

(45) Despiau-Pujo, E.; Davydova, A.; Cunge, G.; Graves, D. B. Hydrogen Plasmas Processing of Graphene Surfaces. *Plasma Chem. Plasma Process.* **2016**, *36*, 213-229.

(46) Yu, Y. J.; Zhao, Y.; Ryu, S.; Brus, L. E.; Kim, K. S.; Kim, P. Tuning the Graphene Work Function by Electric Field Effect. *Nano Lett.* **2009**, *9*, 3430-3434.

(47) Liang, S. J.; Ang, L. K. Electron Thermionic Emission from Graphene and a Thermionic Energy Converter. *Phys. Rev. Appl.* **2015**, *3*, 014002.

(48) Yan, R.; Zhang, Q.; Li, W.; Calizo, I.; Shen, T.; Richter, C. A.; Hight-Walker, A. R.; Liang, X.; Seabaugh, A.; Jena, D.; Xing, H. G.; Gundlach, D. J.; Nguyen, N. V. Determination of Graphene

Work Function and Graphene-Insulator- Semiconductor Band Alignment by Internal Photoemission Spectroscopy. *Appl. Phys. Lett.* **2012**, *101*, 022105.

(49) Mathieu, C.; Barrett, N.; Rault, J.; Mi, Y. Y.; Zhang, B.; De Heer, W. A.; Berger, C.; Conrad, E. H.; Renault, O. Microscopic Correlation between Chemical and Electronic States in Epitaxial Graphene on SiC(000$\bar{1}$). *Phys. Rev. B.* **2011**, *83*, 235436.

(50) Kim, H.; Renault, O.; Tyurnina, A.; Simonato, J. P.; Rouchon, D.; Mariolle, D.; Chevalier, N.; Dijon, J. Doping Efficiency of Single and Randomly Stacked Bilayer Graphene by Iodine Adsorption. *Appl. Phys. Lett.* **2014**, *105*, 222.

(51) Goniszewski, S.; Adabi, M.; Shaforost, O.; Hanham, S. M.; Hao, L.; Klein, N. Correlation of p-Doping in CVD Graphene with Substrate Surface Charges. *Sci. Rep.* **2016,** *6*, 22858.

(52) Kwon, K. C.; Choi, K. S.; Kim, S. Y. Increased Work Function in Few-Layer Graphene Sheets via Metal Chloride Doping. *Adv. Funct. Mater.* **2012**, *22*, 4724-4731.

(53) Kwon, K. C.; Choi, K. S.; Kim, C.; Kim, S. Y. Role of Metal Cations in Alkali Metal Chloride Doped Graphene. *J. Phys. Chem. C* **2014**, *118*, 8187-8193..

(54) Samaddar, S.; Coraux, J.; Martin, S. C.; Grévin, B.; Courtois, H.; Winkelmann, C. B. Equal Variations of the Fermi Level and Work Function in Graphene at the Nanoscale. *Nanoscale* **2016**, *8*, 15162-15166.

(55) Balog, R.; Jørgensen, B.; Nilsson, L.; Andersen, M.; Rienks, E.; Bianchi, M.; Fanetti, M.; Lægsgaard, E.; Baraldi, A.; Lizzit, S.; Sljivancanin, Z.; Besenbacher, F.; Hammer, B.; Pedersen, T. G.; Hofmann, P.; Hornekær, L. Bandgap Opening in Graphene Induced by Patterned Hydrogen Adsorption. *Nat. Mater.* **2010**, *9*, 315-319.

(56) Petit-Etienne, C.; Darnon, M.; Vallier, L.; Pargon, E.; Cunge, G.; Boulard, F.; Joubert, O.; Banna, S.; Lill, T. Reducing Damage to Si Substrates during Gate Etching Processes by Synchronous Plasma Pulsing. *J. Vac. Sci. Technol. B, Nanotechnol. Microelectron. Mater. Process. Meas. Phenom.* **2010**, *28*, 926-934.

(57) Ullal, S. J.; Singh, H.; Daugherty, J.; Vahedi, V.; Aydil, E. S. Maintaining Reproducible Plasma Reactor Wall Conditions: SF_6 Plasma Cleaning of Films Deposited on Chamber Walls during Cl_2/O_2 Plasma Etching of Si. *J. Vac. Sci. Technol. A Vacuum, Surfaces, Film.* **2002**, *20*, 1195-1201.

(58) Escher, M.; Winkler, K.; Renault, O.; Barrett, N. Applications of High Lateral and Energy Resolution Imaging XPS with a Double Hemispherical Analyser Based Spectromicroscope. *J. Electron Spectros. Relat. Phenomena* **2010**, *178*, 303-316.

For Table of Contents Only